Modeling Rapid Flood Propagation Over Natural Terrains Using a Well-Balanced Scheme

Maricarmen Guerra[1]; Rodrigo Cienfuegos, Ph.D.[2]; Cristian Escauriaza, Ph.D.[3]; Fabien Marche, Ph.D.[4]; and José Galaz[5]

Abstract: The consequences of rapid and extreme flooding events, such as tsunamis, riverine flooding, and dam breaks show the necessity of developing efficient and accurate tools for studying these flow fields and devising appropriate mitigation plans for threatened sites. Two-dimensional simulations of these flows can provide information about the temporal evolution of water depth and velocities, but the accurate prediction of the arrival time of floods and the extent of inundated areas still poses a significant challenge for numerical models of rapid flows over rough and variable topographies. Careful numerical treatments are required to reproduce the sudden changes in velocities and water depths, evolving under strong nonlinear conditions that often lead to breaking waves or bores. In addition, new controlled experiments of flood propagation in complex geometries are also needed to provide data for testing the models and evaluating their performance in more realistic conditions. This work implements a robust, well-balanced numerical model to solve the nonlinear shallow water equations (NSWEs) in a nonorthogonal boundary fitted curvilinear coordinate system. It is shown that the model is capable of computing flows over highly variable topographies, preserving the positivity of the water depth, and providing accurate predictions for the wetting and drying processes. The model is validated against benchmark cases that consider the use of boundary fitted discretizations of the computational domain. In addition, a laboratory experiment is performed of a rapid flood over a complex topography, measuring the propagation of a dam break wave on a scaled physical model, registering time series of water depth in 19 cross sections along the flow direction. The data from this experiment are used to test the numerical model, and compare the performance of the current model with the numerical results of two other recognized NSWE models, showing that the current model is a reliable tool for efficiently and accurately predicting extreme inundation events and long-wave propagation over complex topographies. **DOI: 10.1061/(ASCE)HY.1943-7900.0000881.**

Author keywords: Shallow water equations; Shock capturing methods; Well-balanced schemes; Boundary fitted curvilinear coordinates.

Introduction

In recent years, many catastrophic events have involved rapid flooding over complex topography, such as tsunamis and river floods. In Chile, for example, several glacial-lake outburst floods (GLOF) have occurred in Colonia River, a tributary of Baker River (47°10′S; 73°20′ W), as a consequence of the Cachet II lake outburst. In fact, two major events in 2008 generated an increase in the free surface elevation of Baker River above 4.5 m and a peak discharge over 3,000 m^3/s Dirección General de Aguas de Chile (General Water Office of Chile) (DGA) satellite monitoring station at Baker River, Dirección General de Aguas Ministerio de Obras Públicas de Chile (National Water Office of the Public Works Ministry of Chile) (DGA-MOP), Chile), flooding large parts of the Colonia and Baker river valleys and putting at risk the town of Caleta Tortel, located at the mouth of Baker River (Dussaillant et al. 2009). This event has repeated twice a year since 2008, which is likely linked to significant increments of temperature that have been registered on the entire watershed in recent years.

Recently, on February 27, 2010, an 8.8 Mw earthquake occurred off the coast of south-central Chile (Fritz et al. 2011; Lay et al. 2010), generating a destructive tsunami that affected a significant portion of the coast, the Juan Fernández archipelago, and Easter Island, taking the lives of 124 people. As a consequence of these events, local authorities and the central government are currently developing new hazard and risk plans in different coastal communities along Chile, which consider the investigation of the inundation extent and maximum water depth estimations, peak discharge, and velocities, among other hydrodynamic variables for riverine floods and tsunamis.

To study the large and costly consequences of these major rapid flooding events, it is necessary to develop instruments that can be used to accurately and efficiently predict the flow velocities and water depths and to assess their associated hazards and risks. An accurate estimation of flow features such as run-up, affected areas, and arrival time of the peak flood will define better mitigation plans and early warning systems and improve the preparedness of

[1]Research Engineer, Departamento de Ingeniería Hidráulica y Ambiental, Pontificia Universidad Católica de Chile, Av. Vicuña Mackenna 4860, 7820436 Santiago, Chile. E-mail: mnguerra@uc.cl

[2]Associate Professor, Departamento de Ingeniería Hidráulica y Ambiental, Pontificia Universidad Católica de Chile; and Centro Nacional de Investigación para la Gestión Integrada de Desastres Naturales, Av. Vicuña Mackenna 4860, Macul, Santiago 7820436, Chile (corresponding author). E-mail: racienfu@ing.puc.cl

[3]Assistant Professor, Departamento de Ingeniería Hidráulica y Ambiental, Pontificia Universidad Católica de Chile; and Centro Nacional de Investigación para la Gestión Integrada de Desastres Naturales, Av. Vicuña Mackenna 4860, Macul, Santiago 7820436, Chile. E-mail: cescauri@ing.puc.cl

[4]Associate Professor, I3M, Université Montpellier 2, France; and INRIA, équipe LEMON, 34090 Montpellier, France. E-mail: Fabien.Marche@math.univ-montp2.fr

[5]Undergraduate Student, Departamento de Ingeniería Hidráulica y Ambiental, Pontificia Universidad Católica de Chile, Av. Vicuña Mackenna 4860, 7820436 Santiago, Chile. E-mail: jdgalaz@uc.cl

Note. This manuscript was submitted on April 7, 2013; approved on February 4, 2014; published online on March 17, 2014. Discussion period open until August 17, 2014; separate discussions must be submitted for individual papers. This paper is part of the ***Journal of Hydraulic Engineering***, © ASCE, ISSN 0733-9429/04014026(11)/$25.00.

people when facing such catastrophic situations, incorporating hydrodynamic forces into the design of coastal and riverine infrastructure (FEMA 2011; ASCE 2006; Yeh 2006).

Nonlinear shallow water equations (NSWEs) are usually employed in these cases to describe the flow dynamics and to model fairly long waves in a homogeneous and incompressible fluid. They are obtained by vertically averaging the three-dimensional Navier-Stokes equations assuming a hydrostatic pressure distribution, resulting in a set of horizontal two-dimensional hyperbolic conservation laws that describe the evolution of the water depth and depth-averaged velocities (Cunge et al. 1980; Stoker 1992).

In the last decades, a significant number of numerical models have been developed to simulate these complex flows, employing finite-difference methods (Molls and Chaudry 1995; Molls and Zhao 2000), finite-element methods (Berger and Stockstill 1995; Tucciarelli and Termini 2000), or finite-volume methods (Valiani et al. 2002; Zhou et al. 2004; Loose et al. 2005). In the framework of finite-volume methods, Godunov-type formulations are very useful to solve the NSWEs, because they can reproduce complex discontinuities such as shockwaves or wet–dry interfaces by solving a Riemann problem at each cell interface of the discretized domain (Toro 2001; LeVeque 2002).

Many environmental flows such as bore propagation (Hibberd and Peregrine 1979), tsunami inundations (Yeh 1991), or glacial lake outburst floods (Cenderelli and Wohl 2001) fall within this category of extreme flood events that can be represented by the NSWEs. They are characterized by rapid wetting and drying over highly variable topographies, giving rise to complex unsteady free surface dynamics that pose a significant challenge for the numerical models. Numerical strategies for integrating the governing equations in these shallow, extreme flows must also address complicated geometries and the highly complex dynamics of wave breaking and run-up. Similarly, the discretization of the boundaries of the physical domain may have a strong influence on the development of the flow dynamics, introducing errors or numerical instabilities if not carefully performed (Baghlani et al. 2008).

Motivated by these applications, this investigation develops an efficient numerical model to solve the two-dimensional dynamics of extreme flows over natural terrains. The method of Marche et al. (2007) is extended, which has resolved complex features of free-surface flows by implementing a well-balanced approach. Well-balanced schemes are specifically conceived to preserve local and global mass conservation to machine accuracy, maintaining steady and motionless states. To achieve this requirement, it is necessary to carefully discretize the friction and bed-slope source terms [more details are provided by Greenberg and Leroux (1996), LeVeque (1998); Gallouet et al. (2003), Audusse et al. (2004), Liang and Marche (2009)]. The governing equations are formulated and solved in a nonorthogonal generalized curvilinear coordinate framework to model the propagation of extreme flows over natural terrains. A finite volume well-balanced approach is used, based on a robust VFRoe (Masella et al. 1999)-relaxation Riemann solver (Gallouet et al. 2003; Berthon and Marche 2008), calculating mass and momentum fluxes at cell interfaces and performing the hydrostatic reconstruction method proposed by Audusse et al. (2004). The source term that accounts for friction effects is treated with the semi-implicit fractional step approach of Liang and Marche (2009). Validation of the new model is presented through comparison with benchmark tests, which are specifically chosen to assess the ability of the model to address wet–dry interfaces, complex geometries, shocks, friction, and bathymetric source terms.

In addition, the future studies of these flows will require new experiments, representing the complex features of rapid flooding events over realistic arbitrary geometries, to test and improve the numerical models. This investigation also includes a dam break experiment on a scaled physical model, representing the bed and banks of a mountain river. Time series of water depth are registered and the results are compared with simulations conducted by using the new, well-balanced numerical model, showing that it can capture the most relevant characteristics of the flow. Furthermore, to compare the performance of the current model with previously validated numerical models, this experience is simulated by using two well-known shock-capturing NSWE models, *ANUGA* (Mungkasi and Roberts 2013) and *GeoClaw* (Berger et al. 2011). From this comparison, the improvements achieved by the new numerical approach can be established in terms of the overall agreement of the free surface variations in time, the estimation of the maximum amplitude of the propagated bore, and its arrival time to different locations.

The paper is organized as follows: the next section presents the nondimensional governing equations and the partial transformation to generalized nonorthogonal curvilinear coordinates that are employed in the model. The numerical scheme and different algorithms used to integrate the NSWEs are briefly described in the third section. Validation tests and comparisons of numerical simulations with benchmark cases and previously published experimental data are presented in the fourth section. The penultimate section describes new dam break experiments conducted in the Hydraulic Laboratory of the Pontificia Universidad Católica de Chile, intended to further validate the model over a realistic and highly variable topographic configuration. Conclusions and future perspectives of this work are discussed in the final section.

Governing Equations

The two-dimensional NSWEs represent a system of nonlinear partial differential equations representing the mass and momentum conservation laws, which were originally derived by Saint-Venant (1971). The fluid is assumed to be incompressible and homogeneous, with hydrostatic pressure distribution. The shallow water or long-wave hypothesis considers negligible vertical velocities and depth-uniform horizontal velocities. Hence, the NSWEs are often applied to river or near-shore flows where the characteristic horizontal wavelength is much longer that the characteristic water depth [more details are provided by Cunge et al. (1980)].

The following will work with a nondimensionalized set of NSWEs by choosing characteristic horizontal and vertical length scales and a velocity scale ($\mathcal{L}$, $\mathcal{H}$;, and $\mathcal{U}$, respectively). By defining the length and velocity scales of the flow, the time scale is represented by $T = \mathcal{L}/\mathcal{U}$, and the dimensionless Froude number by $\mathsf{F} = \mathcal{U}/\sqrt{g\mathcal{H}}$, which quantifies the relative importance of inertial effects over gravity (g). The dimensional variables, noted with a hat ($\widehat{\ }$), are hereafter defined as $\widehat{x} = \mathcal{L}x$, $\widehat{y} = \mathcal{L}y$, $\widehat{z} = \mathcal{H}z$, $\widehat{h} = \mathcal{H}h$, $\widehat{u} = \mathcal{U}u$, $\widehat{v} = \mathcal{U}v$, and $\widehat{t} = Tt$, where $\widehat{x}$ and $\widehat{y}$ represent the Cartesian directions, $\widehat{z}$ defines bed elevation, $\widehat{h}$ is water depth, $\widehat{u}$ and $\widehat{v}$ are the depth-averaged flow velocities in each Cartesian direction, and $\widehat{t}$ is time. To better reproduce complex arbitrary geometries, a boundary fitted curvilinear coordinate system is introduced in two dimensions, denoted by the system (ξ, η). Generalized curvilinear coordinates are chosen to follow the boundaries of the physical domain, adapting the grid to the geometrical details of the terrain. This transformation provides better resolution in zones of interest and an accurate representation of the boundaries, resulting in an efficient discretization of the flow domain (Lackey and Sotiropoulos 2005; Liang et al. 2007; Baghlani et al. 2008).

The Cartesian NSWEs can be partially transformed to this new coordinate system, maintaining the hydrodynamic variables

referenced to the Cartesian frame. This procedure is known as partial transformation and only modifies the mass and momentum fluxes of the governing equations. The full transformation would change the hydrodynamic variable vectors, $Q = [h, hu, hv]^T$, to the velocity components in the ξ and η directions, using the so-called contravariant velocity components, and the derivatives in the convective terms would yield the well-known Christoffel symbols of the second kind (Ahn and Hosoda 2007). Therefore, considering only bed slope and friction source terms, the nondimensional NSWEs can be written in curvilinear coordinates in the following form (Lackey and Sotiropoulos 2005):

$$\frac{\partial Q}{\partial t} + J\frac{\partial F}{\partial \xi} + J\frac{\partial G}{\partial \eta} = S_b(Q) + S_f(Q) \tag{1}$$

where Q = vector of hydrodynamic variables; F and G = flux vectors expressed in terms of the new spatial coordinate system ξ and η, respectively; $S_b(Q)$ and $S_f(Q)$ = source term vectors. These vectors are given by the following expressions:

$$Q = \begin{pmatrix} h \\ hu \\ hv \end{pmatrix}, \quad F = \frac{1}{J}\begin{pmatrix} hU^1 \\ uhU^1 + \frac{1}{2Fr^2}h^2\xi_x \\ vhU^1 + \frac{1}{2Fr^2}h^2\xi_y \end{pmatrix},$$

$$G = \frac{1}{J}\begin{pmatrix} hU^2 \\ uhU^2 + \frac{1}{2Fr^2}h^2\eta_x \\ vhU^2 + \frac{1}{2Fr^2}h^2\eta_y \end{pmatrix},$$

$$S_b(Q) = \begin{bmatrix} 0 \\ -\frac{h}{Fr^2}(z_\xi\xi_x + z_\eta\eta_x) \\ -\frac{h}{Fr^2}(z_\xi\xi_y + z_\eta\eta_y) \end{bmatrix}, \quad S_f(Q) = \begin{pmatrix} 0 \\ -\tau_{fx} \\ -\tau_{fy} \end{pmatrix} \tag{2}$$

where h = water depth; u and v = nondimensional depth-averaged flow velocities in each Cartesian direction; z = bed elevation; z_ξ and z_η = local bed slope with respect to the transformed coordinate system (ξ, η); and S_f = friction source term.

The additional terms that appear in the fluxes, ξ_x, ξ_y, η_x, and η_y, are the resulting metrics associated to the coordinate changes, and $J = \xi_x\eta_y - \xi_y\eta_x$ is the Jacobian of the transformation, which will remain constant for a fixed grid. Also, U^1 and U^2 are the contravariant velocity components, expressed as $U^j = u\epsilon_x + v\epsilon_y$ with $(j, \epsilon) \in \{(1, \xi), (2, \eta)\}$ The transformed system of equations is discretized on a rectangular and uniform grid in the transformed space (ξ, η) using the finite-volume method that is described in the next section.

Numerical Scheme

The curvilinear NSWE system given in Eq. (1) is integrated by using a well-balanced finite-volume scheme, coupled with a splitting strategy for the treatment of source terms (Liang and Marche 2009). The solution associated to the system of Eq. (1) is decomposed at each time step by solving two systems, one associated with the NSWEs with topography source terms and a second associated with the remaining friction terms. The following subsections describe the different steps of the algorithm, including the implementation of the boundary conditions, and the stability criterion of the numerical solution.

Solution of the NSWEs with Topography Source Terms

This step solves the following system associated with the NSWEs with topography source terms:

$$\frac{\partial Q}{\partial t} + j\frac{\partial F}{\partial \xi} + J\frac{\partial G}{\partial \eta} = S_b(Q) \tag{3}$$

A numerical strategy is sought that provides stable shock-capturing integration of Eq. (3) with precise control of the spurious oscillations induced by numerical dispersion. In addition, the scheme should be able to handle the complex interactions between flow and topography, including the preservation of motionless and steady states. It was chosen to adapt the robust second-order finite-volume scheme introduced by Marche et al. (2007) to the non-orthogonal boundary fitted coordinate framework.

Taking into account the new system of coordinates, the spatial discretization of Eq. (3) can be recast under the following semidiscrete finite-volume formalism:

$$\frac{d}{dt}Q_{i,j} + \frac{J_{i,j}}{\Delta\xi}(F^*_{i+(1/2),j} - F^*_{i-(1/2),j}) + \frac{J_{i,j}}{\Delta\eta}(G^*_{i,j+(1/2)} - G^*_{i,j-\frac{1}{2}}) = S_{b(i,j)} \tag{4}$$

where $Q_{i,j}$ = vector of cell-centered hydrodynamic variables; $J_{i,j}$ = cell-centered Jacobian of the coordinate transformation; $F^*_{i\pm1/2,j}$ and $G^*_{i,j\pm1/2}$ = numerical flux functions through the (i, j) cell interfaces; and $S_{b(i,j)}$ = centered discretization of the bed-slope source term. The cell sizes are denoted by $\Delta\xi$ and $\Delta\eta$, and the interface between the (i, j)th cell and the $(i + 1, j)$th is denoted by $(i + \frac{1}{2}, j)$, as depicted in Fig. 1.

The computation of the numerical fluxes $F^*_{i\pm1/2,j}$ and $G^*_{i,j\pm1/2}$ is achieved by using a robust VFRoe relaxation scheme proposed by Gallouet et al. (2003). To achieve a second-order accurate scheme, the monotonic upstream scheme for conservation laws (MUSCL) extrapolation proposed by Van Leer (1979) is straightforwardly applied. This technique considers that numerical fluxes are computed by linearly reconstructing the hydrodynamic variables, leading to more accurate reconstructed states at each side of the interface of every cell, as shown in Fig. 1 [details are provided by Bouchut (2004)]. To handle topographic variations and the requirement for the preservation of static flows, the well-balancing discretization for the bed-slope term proposed by Audusse et al. (2004) was also adapted to the boundary fitted curvilinear coordinate system of equations. In this step of the algorithm, a linear reconstruction of the topography was built considering the MUSCL reconstructed hydrodynamic variables, as shown in Marche et al. (2007). Finally, the source term $S_b(Q)$ is estimated through the new reconstructed values of the fluxes. A detailed description of the computation of the fluxes and the hydrodynamic variables is provided in the work of Marche et al. (2007) and Berthon and Marche (2008).

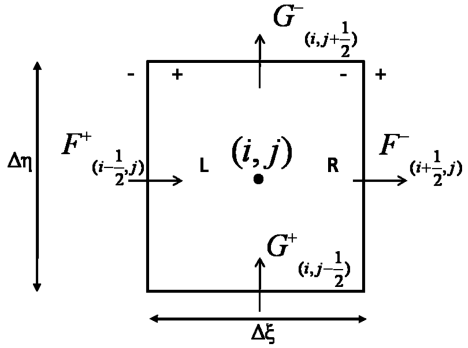

Fig. 1. Discretization cell and numerical fluxes ("L" and "R" denote the left and right boundaries of the cell; plus and minus signs represent the left and right sides of the cell interface)

J. Hydraul. Eng.

Solution of the Friction Source Terms

The friction source term is incorporated by using the splitting semiimplicit method proposed by Liang and Marche (2009). The corresponding ordinary differential equation of the splitting operation is defined as follows:

$$\frac{dQ}{dt} = S_f \tag{5}$$

where

$$S_f = (0, -\tau_{fx}, -\tau_{fy})^T \tag{6}$$

In this equation, the terms τ_{fx} and τ_{fy} = nondimensionalized bed shear-stresses for each Cartesian direction. The magnitude of the bed shear stresses in each direction can be calculated as follows:

$$\tau_{fx} = C_f u\sqrt{u^2 + v^2} \tag{7}$$

$$\tau_{fy} = C_f v\sqrt{u^2 + v^2} \tag{8}$$

where C_f = nondimensionalized bed friction coefficient, which can be expressed by using one of the standard existing approaches developed for uniform flows, such as Manning or Chézy. Following the algorithm developed by Liang and Marche (2009), Eq. (5) is integrated by using an implicit scheme and a second-order Taylor series expansion. An additional friction limitation may be locally added to prevent unphysical flow from reversing, owing to large drag forces in vanishing depth areas, as mentioned by Burguete et al. (2008).

As far as time discretization is concerned, a classical second-order Runge-Kutta scheme is used for each time-step in this splitting approach. To solve system shown in Eq. (1) at the boundaries of the computational domain, three types of boundary conditions have been implemented and tested in the model: (1) transmissive or open boundary, allowing the information to freely leave the domain without propagating spurious information back to the domain; (2) solid wall or close boundary, which imposes no discharge through the boundary of the domain; and (3) absorbing/generating boundary condition, which relies on the work of Sanders (2002) and Cienfuegos et al. (2007) and allows inflow discharge or free surface information at the boundary to be prescribed, such as incoming waves or stage-discharge relationships, and back-traveling waves to be freely evacuated. Finally, the stability of the numerical model is controlled by the Courant-Friedrich-Lewy criterion (CFL) (Toro 2001).

Validation

As previously explained, the numerical model in nonorthogonal generalized coordinates is based on the method of Marche et al. (2007), incorporating bed friction with the splitting semiimplicit method of Liang and Marche (2009). Initially, the model was validated by using various benchmark cases that are not shown herein, for rectangular domains employing discretizations in Cartesian coordinates. These first tests involved shock-capturing and moving shoreline problems, quantitatively determining accurate results in comparison with analytical solutions and laboratory data; these are the same cases previously studied by Marche et al. (2007). The following series of benchmark tests are intended to illustrate the improvements obtained when a boundary fitted curvilinear discretization is used, and to prove the ability of the model to deal with complex geometries, bed slope, and friction source terms.

Dam Break in a Convergent–Divergent Flume

The numerical model is tested with a dam break induced flow in a convergent–divergent channel, performing simulations of two-dimensional flood waves studied experimentally by Bellos et al. (1992). The channel is 21.2 m long and has a rectangular cross section of variable width. At a distance of 5 m downstream from the beginning of the flume, there is a smooth curved contraction and expansion with minimum width of 0.6 m; the flume has a constant bed slope that can be changed and ranges between $\pm 1\%$. A detailed description of the domain is provided in the work of Bellos et al. (1992).

The simulation of the experiment is conducted by using a nonuniform boundary fitted mesh of 241×41 cells; the channel is assumed to have a mild bed slope, $S_0 = 0.002$, and a Manning friction coefficient $n = 0.012$, consistent with the recommendations of Bellos et al. (1992). The dam is located at the end of the contraction, at a distance of 8.5 m from the upstream boundary of the flume. Initial conditions consist of a water depth of 0.30 m upstream of the dam, null flow velocities, and dry terrain downstream of the dam. A no-flow boundary condition is imposed at the sidewalls and at the upstream boundary of the flume. At the downstream end of the channel, an open boundary condition is applied to allow all information to exit the domain without propagating back and perturbing the numerical solution. The simulations are conducted for 70 s by using a CFL number equal to 0.9 to ensure numerical stability during the computations. The geometry of the channel, dimensions, and locations of measurement points studied by Bellos et al. (1992), along with the computational mesh, are shown in Fig. 2.

The results show that dam break phenomena are correctly captured by the numerical model, as shown in Fig. 3. At the breaking,

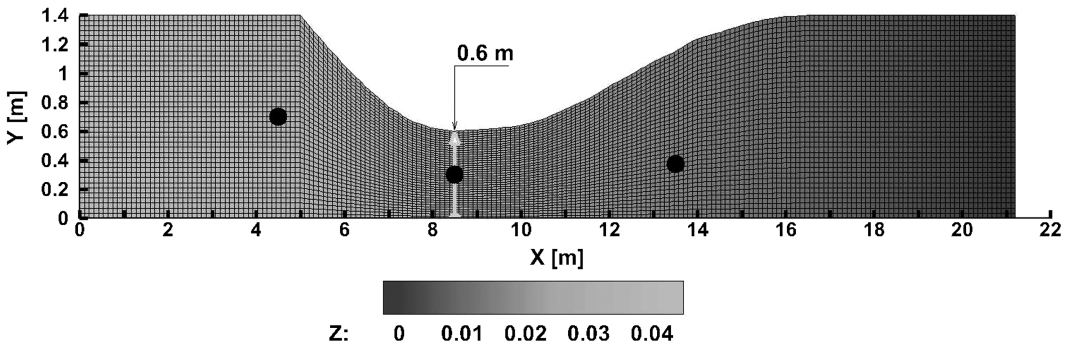

Fig. 2. Dam break in a convergent–divergent flume: geometry of the channel, boundary fitted grid, bathymetry, and measurement points (black dots)

J. Hydraul. Eng.

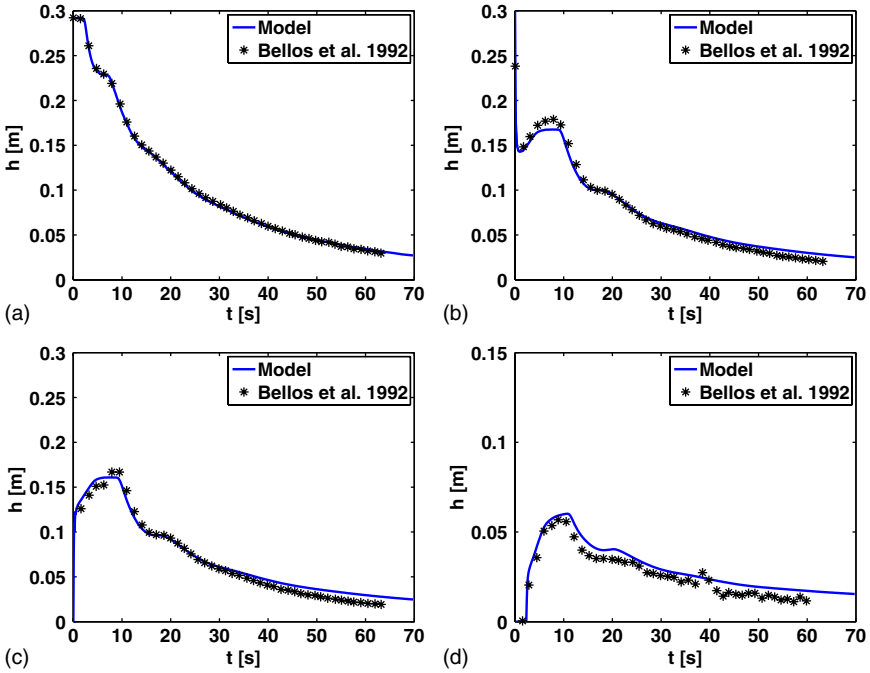

Fig. 3. Dam break in a convergent–divergent flume showing water depth time series at measurement points: (a) $x = 4.0$ m; (b) $x = 8.5^{-}$ m; (c) $x = 8.5^{+}$ m; (d) $x = 13.5$ m

the shock wave spreads through the expansion and propagates downstream, inundating the dry bottom. A rarefaction wave propagates upstream, decreasing the water depth, which is reflected at the upstream closed boundary of the flume. Then, the water depth in the flume starts decreasing, reaching a minimum of 0.014 m after 70 s. The images depicted in Fig. 3 show that computed water depths and arrival times of the front are in excellent agreement with experimental data for all measurement points in the study, confirming the abilities of the model to capture shocks and handle wet–dry cells and source terms over a curvilinear geometry.

Dam Break over a Closed Basin with Steep Topography and Friction

An important characteristic of the model is its capability of handling frictional source terms in the numerical solution of the NSWEs, especially for situations in which the flow is shallow or the process of wave run-up/run-down is important. Here, the numerical model is tested with a flood produced by a dam break over a closed channel with three conical obstacles. This test was first proposed by Kawahara and Umetsu (1986) and subsequently used by many researchers (Brufau et al. 2002; Brufau and García-Navarro 2003; Gallardo et al. 2007; Nikolos and Delis 2009) to assess the ability of numerical models to address steep bed slopes and friction source terms and wetting/drying proceses, and to test local and global mass conservation.

The basin is 70 m long in the streamwise x-direction and 30 m wide in the cross-stream or y-direction. The topography of the bed is defined by the following equation:

$$z(x,y) = \max \begin{bmatrix} 0 \\ 1 - 0.1 \times \sqrt{(x-30)^2 + (y-22.5)^2} \\ 1 - 0.1 \times \sqrt{(x-30)^2 + (y-7.5)^2} \\ 2.8 - 0.28 \times \sqrt{(x-47.5)^2 + (y-15)^2} \end{bmatrix} \quad (9)$$

Initial conditions consist of a motionless free surface elevation upstream of the dam location (at $x = 16$ m) equal to 1.82 m, and a dry bottom bed downstream. The simulation is performed by employing a 101×101 uniform mesh using the suggested Manning coefficient of $n = 0.018$, and no-flow boundary conditions are applied to all sidewalls of the basin. Computations are conducted for 400 s to achieve steady state, as shown in previous investigations (Nikolos and Delis 2009), using a CFL number equal to 0.9 to ensure the stability of the model during these computations. Evolution of the free surface is shown in Fig. 4. After the dam break, the flood wave wets the small obstacles and a reflected wave is propagated back to the upstream boundary. At the same time, the front passes through the small obstacles and runs up and down over the larger obstacle, which is partially dry. Later, the wetting front separates and symmetrically goes around the larger mound as it crosses back at the middle of the channel downstream from the larger conical obstacle. Finally, the wave hits the downstream solid boundary and is reflected back to the obstacles. The motion decays in time as a consequence of the friction force; after approximately 400 s, the steady state is reached, leaving the three obstacles partially dry. These results agree with those obtained by Gallardo et al. (2007) and Nikolos and Delis (2009), and illustrate the ability of the model to accurately represent the interaction between dry and wet cells over a steep and frictional topography. Results also demonstrate that global mass conservation is achieved during the entire computation. Therefore, the robustness and stability of the friction scheme in conjunction with the well-balancing properties of the solution of the hyperbolic system are validated.

Experimental Dam Break over Complex Terrain and Numerical Simulation

With the purpose of testing the numerical model, an experiment is conducted for the propagation of a dam break wave generated by the rapid emptying of a reservoir over a scaled physical model of a river. The experiments are conducted in the Hydraulic Laboratory of the Pontificia Universidad Católica de Chile. This section presents the details of the experiment and the comparison between

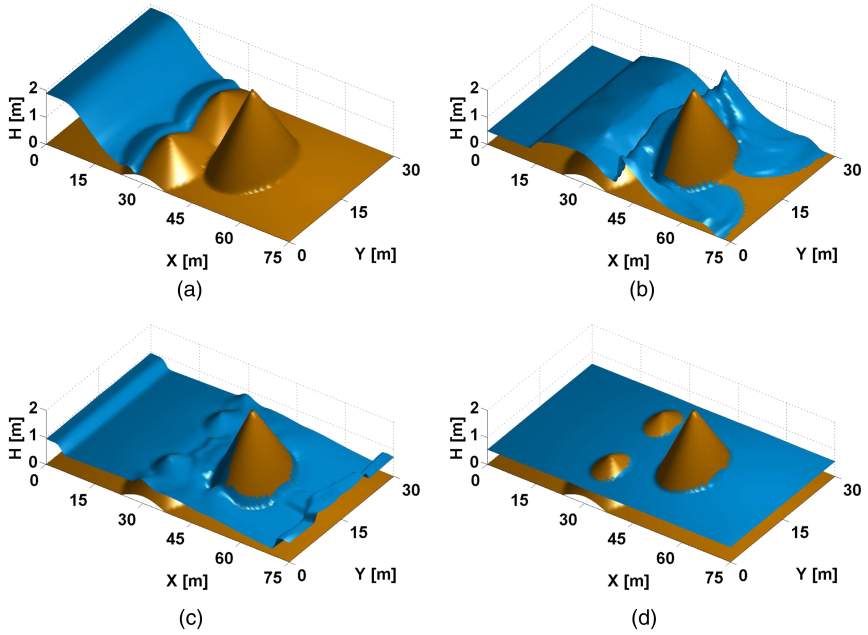

Fig. 4. Dam break over a closed basin showing free surface elevation: (a) $t = 2$ s; (b) $t = 12$ s; (c) $t = 20$ s; (d) $t = 300$ s

experimental results and numerical solutions obtained with the current model and with two recognized NSWE models: *ANUGA* (Mungkasi and Roberts 2013) and *GeoClaw* (Berger et al. 2011), showing the capacity of the models to handle highly demanding natural conditions analogous to the propagation of a tsunami wave over varying topography.

Experimental Setup

Dam break experiments are conducted in a physical model of a river consisting of a narrow and steep valley with complex topography, presented in Fig. 5(a). The model is built by using Froude similarity and a geometrical scale equal to 1:60. The entire river reach is 14.6 m long and has a maximum width of 4.5 m. It starts with a narrow and curved zone with an average adverse bed slope of nearly −4.5%, then becomes wider toward its downstream end. The average bed slope over the river reach considered in the experiments is −1.5%. A longitudinal profile of the river reach, along with the locations of the measurement points, is shown in Fig. 5(b). The river bed includes a uniform concrete mix with fine gravel, which yields roughness characterized by a Manning coefficient of $n = 0.014$.

Upstream of the river reach, there is a reservoir and a wooden gate that holds a fixed volume of water equal to 2.17 m^3 . The experiment consists of a sudden lift of the reservoir gate to release the water into a quiescent free surface downstream. A bore wave is produced and propagated to the end of the river reach. The free surface evolution within the scaled model is recorded during 60 s. At the reservoir, free surface elevation is set at 0.85 m, whereas at the river, it is set at 0.56 m, as shown in Fig. 5(b). Free surface variations are recorded at 19 points in the river reach and at the reservoir, as depicted in Fig. 5(b).

At the reservoir, free surface variations are measured by using a KPSI (Measurement Specialties, Hampton, Virginia) brand pressure transducer recording voltage at 100 Hz. The accuracy of this instrument is ±1% and it is calibrated such that 1 V equals 1 m of water column. At downstream cross sections, free surface variations over the mean water level are measured by using wave Danish Hydraulic Institute (DHI) resistive gauges, which were located at the thalweg of

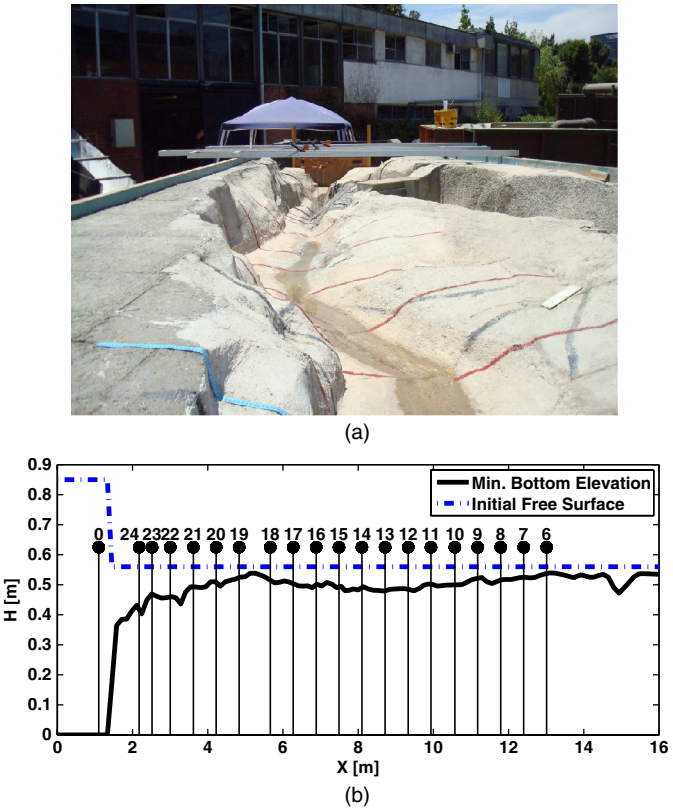

Fig. 5. Dam break experience: (a) physical model and measurement instruments, upstream view; (b) longitudinal profile of the bottom elevation of the river reach, initial conditions, and measurement points

the cross sections under investigation. Each gauge records voltage data at 100 Hz; the accuracy of these gauges is ±1.5 mm and the zero drift is ±5%, depending on the water temperature. For the experiments, four resistive gauges are used, i.e., only four points can be measured at each run. Thus, five set of experiments with different

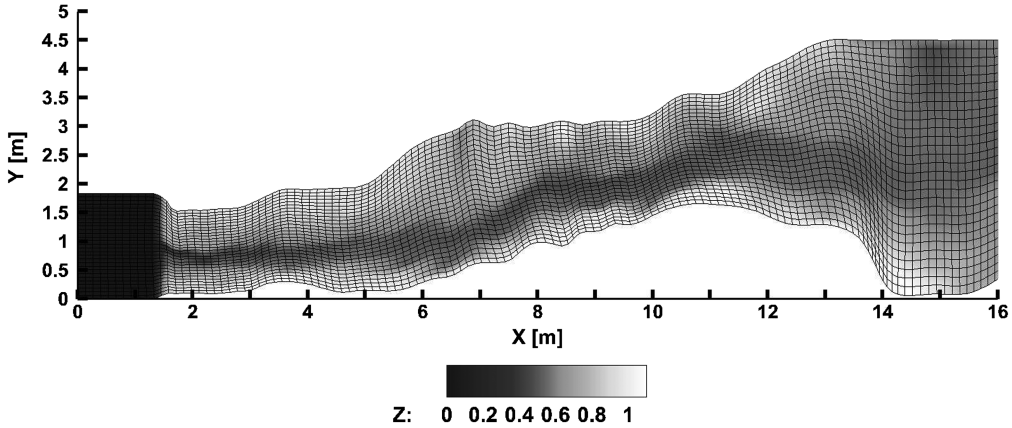

Fig. 6. Numerical model of dam break experience: digital bathymetry of the physical domain and curvilinear mesh of the physical model of 130×30 cells

gauge positions are performed to cover the 19 sections under consideration. As a verification of the repeatability of the data, three repetitions are performed at each gauge location, maintaining the position of the pressure sensor in the reservoir to use it as a reference to synchronize the time series.

Numerical Simulation

The digitized bathymetry of the physical model is constructed from 39 cross sections measured within the river reach. Next, the bathymetric data, together with the reservoir geometry, is interpolated by using a cubic spline method to create a boundary fitted computational domain, which correctly represents the bathymetric features of the river reach and its geometry. The physical model is discretized into 130×30 cells of variable size, covering an area of 16×4.5 m^2. The mesh used in the simulations and the digitized bathymetry are shown in Fig. 6. As initial conditions, free surface elevations at the reservoir and the river are set to 0.85 m and 0.56 m, respectively. Zero velocities over the entire domain are considered at $t = 0$. The open boundary condition is used at the downstream end of the river reach and closed boundary conditions are applied to the sides of the computational domain. CFL condition is set to 0.9 to ensure the numerical stability of the simulations. The gate is instantly removed at $t = 0$ and the wave propagates downstream, as shown in the experiments.

Results

The numerical model is able to simulate the dam break event and the propagation of the bore wave over the river reach. Fig. 7 illustrates the propagation process, showing four snapshots of the numerical computation, in which blue represents the wet surface. As depicted in these figures, the bore propagates downstream of the river reach through the narrow and steep valley. It takes approximately 10 s for the bore wave to reach the end of the river reach ($\approx$ 14 m). The entire flood wave propagates downstream along the complex geometry of the physical model, flooding and drying cells, and reaches steady state after nearly 60 s. Fig. 8 shows the velocity

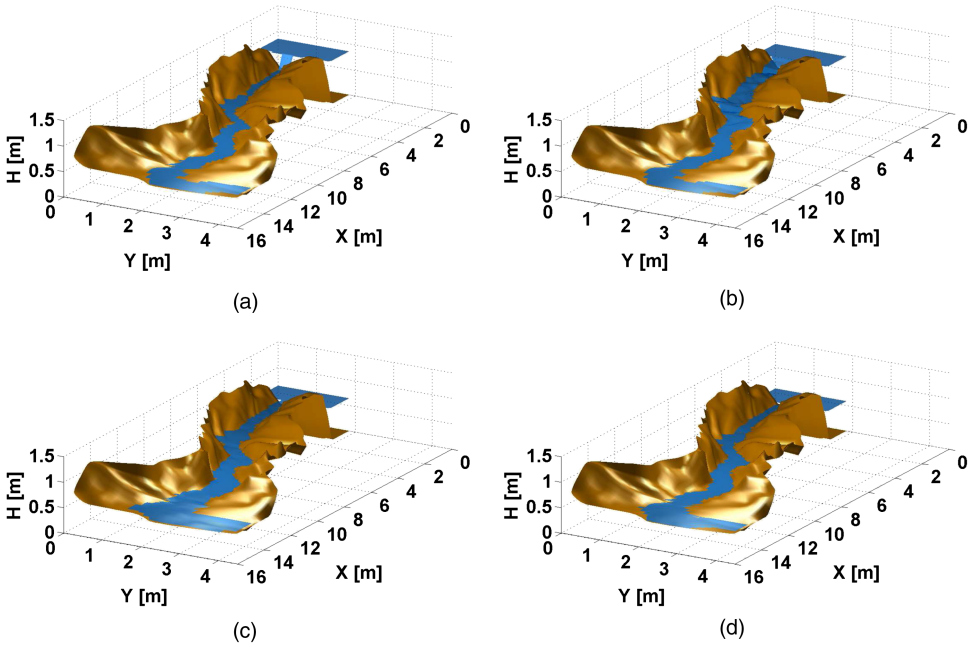

Fig. 7. Numerical model of dam break experience showing flood extension at different times: (a) initial condition; (b) $t = 4.4$ s; (c) $t = 20$ s; (d) $t = 60$ s

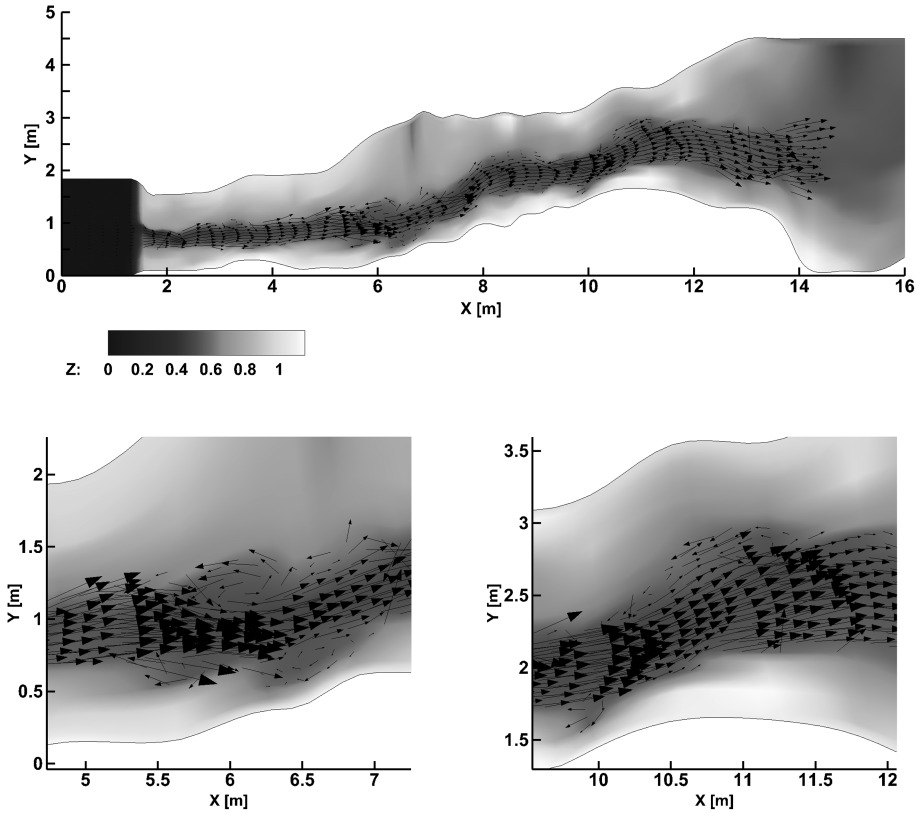

Fig. 8. Numerical model of dam break experience: velocity vectors for the propagation of the flooding wave over the river at $t = 10$ s

vectors field 10 s after the gate opening; flow features determined in the laboratory experiments, such as recirculation and reflection owing to topographical obstacles, are observed in these numerical results. Thus, the primary aspects of the rapidly varying flow measured in the experiments are reproduced by the numerical model.

Evolution of the bore wave is studied and compared to experimental data through time series of the computed free surface dynamics at the same locations measured in the experiments. Additionally, numerical simulations are conducted by using similar NSWE numerical models to assess and compare the accuracy of the current model for similar discretization settings. The chosen numerical models are *ANUGA* (Mungkasi and Roberts 2013) and *GeoClaw* (Berger et al. 2011). Both models solve the NSWE by using a well-balanced shock capturing finite-volume method, primarily differing in the discretization of the domain; *ANUGA* uses nonstructured meshes, whereas *GeoClaw* uses an adaptive meshing approach. To define comparable grids for both simulations, meshes are prepared with similar discretization sizes. For *ANUGA*, a mesh is defined of 4,026 triangular elements. *GeoClaw* uses an adaptive mesh configuration that varies the distribution of element size with time, defining areas of refinement when needed. For this particular case, the refinement zone is controlled to mantain a number of grid nodes similar to the current model and to *ANUGA*. Figures showing the defined grids for *ANUGA* and *GeoClaw*, along with the configuration for both simulations, are presented in the appendix.

Comparisons between measured and computed time series of the free surface evolution for the three models are presented in Fig. 9. The analysis shows that the primary features of the process, i.e., the arrival times, peak amplitudes and recession curves, are well reproduced by the current numerical model and by *GeoClaw*. *ANUGA* results seem to be accurate in representing maximum amplitude, but for this particular case, the model overestimates the final free surface elevation.

Based on the results obtained in the simulations, three quantities are established related to the inundation and propagation processes in the study: the overall agreement of the free surface elevation with time, the maximum amplitude of the bore at each measurement location, and the arrival time of the wave front. For each of these variables, mean relative errors to the measurements are calculated at gauge locations; these relative errors are defined as described in the following subsections.

Relative Root Mean Square Error

A root mean square error is used to compare the experimental and numerical free surface elevations at each location and to highlight the locations where larger differences are found. The relative root mean square error (RRMSE) for a location k, and the average RRMSE considering all locations are defined, respectively, as

$$\mathrm{RRMSE}_k^2 = \frac{1}{T}\int_0^T \left[\frac{\eta_m^k(t) - \eta_n^k(t)}{\eta_m^k(t)}\right]^2 dt \tag{10}$$

$$\mathrm{RRMSE} = \left(\frac{1}{M}\sum_{k=1}^{n} \mathrm{RRMSE}_k^2\right)^{1/2} \tag{11}$$

where T = period of time considered in measurements and simulations (60 s); M = number of measurement points; and η_m^k and η_n^k = measured and numerical free surface elevation at each k location, respectively.

Maximum Amplitude of the Wave

The maximum amplitude of the bore is an important flood variable because it is related to the destructive potential of the wave. This variable is defined as the difference between the maximum and the initial free surface elevations at the river reach. The mean relative error between experimental data and numerical results is estimated as follows:

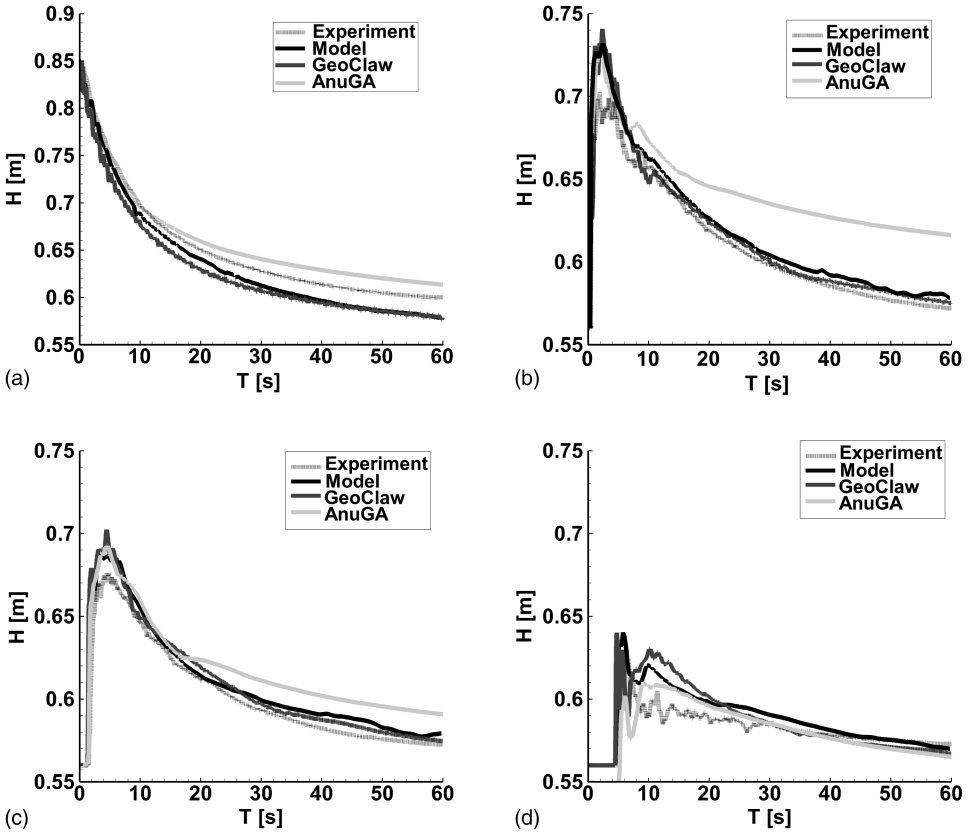

Fig. 9. Numerical model of dam break experience showing comparison between measured and predicted free surface elevation at different locations: (a) reservoir; (b) Gauge Location 24; (c) Gauge Location 20; (d) Gauge Location 12 (in all figures, the dotted black line represents the experiments and the solid lines represent the numerical results of the current model, *GeoClaw*, and *ANUGA*)

$$\Delta H_r = \frac{1}{M}\sum_{k=1}^{M}\left|\frac{H(\eta_m^k) - H(\eta_n^k)}{H(\eta_m^k)}\right| \tag{12}$$

Arrival Time

The arrival time of the wave is an interesting parameter for defining evacuation plans because it indicates the available time to leave flood-prone areas and is a proxy for the celerity of the bore. The arrival time of at location k is defined as the first instant at which the signal surpasses the initial value by a certain threshold, which is defined here as 1 mm. The mean relative error of this variable over all measuring sections is defined as

$$\Delta T^a = \frac{1}{M}\sum_{k=1}^{M}\left|\frac{T^a(\eta_m^k) - T^a(\eta_n^k)}{T^a(\eta_m^k)}\right| \tag{13}$$

The calculated mean relative errors for each model are summarized in Fig. 10. The RRMSE for the three models agrees very well overall between measurements and numerical predictions, with a 1.7% relative error for the current model and a 2.1 % relative error for *ANUGA* and *GeoClaw*, which is an acceptable error, considering the demanding nature of the experiment. For the current model, the highest relative errors are found in the gauges located upstream, near the gate.

It is found that, on average, the maximum amplitude is underestimated by all models because it is the variable with the highest relative error. However, in terms of arrival times of the wave front, predicted results are in excellent agreement with observations (less than 5% mean relative error for the current model). The primary differences are found in the first gauges closest to the reservoir, with maximum local errors reaching 10%. These differences may be explained by the opening mechanism of the gate, which

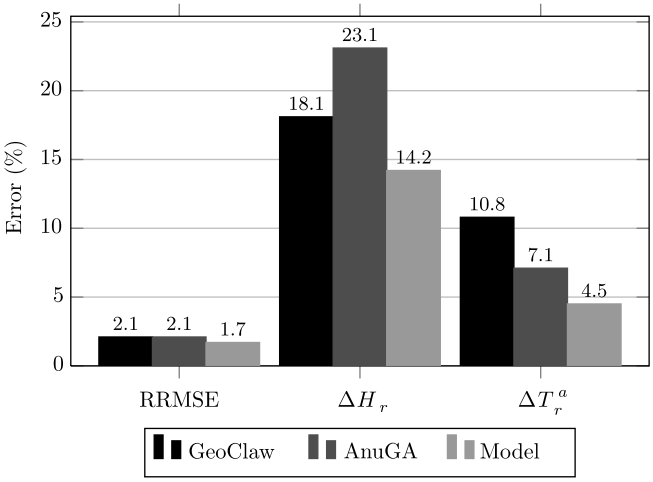

Fig. 10. Summary of mean relative errors between experiments and numerical results for each NSWE model (RRMSE: relative root mean square error between experimental and numerical free surface elevation; ΔH_r: mean relative error in the maximum amplitude of the bore; ΔT_r^a: mean relative error in the arrival time of the bore)

is frictionless and instantaneous in the simulation, but performed in a finite time in the experiments; here, vertical velocities may also be generated and interfere with the dynamics of the wave downstream, thus increasing the maximum amplitude of the wave.

Summarizing, the results from the current model show that it can correctly capture the time evolution of the free surface elevation,

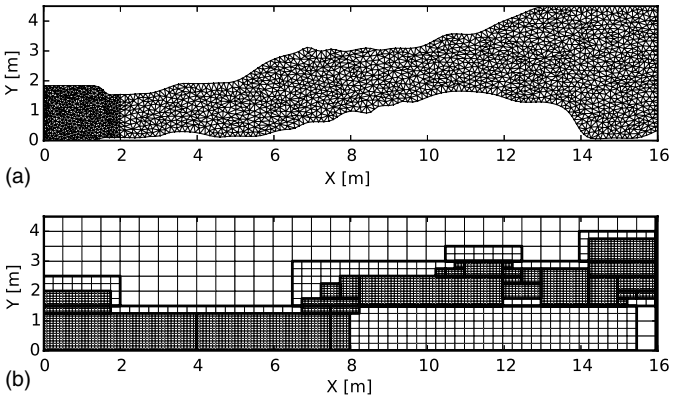

Fig. 11. Physical model discretization grids: (a) triangular mesh of 4,060 elements for *ANUGA*; (b) initial adaptive mesh with three levels of refinement for *GeoClaw*

the arrival time of the bore, and its maximum amplitude. For this singular case, simulations show a decrease in the relative errors when compared to the results of previously validated numerical models when a similar discretization setting of the domain is used.

Conclusions

This investigation developed and validated a finite-volume numerical model to simulate extreme flows and rapid flooding over natural terrains and complex geometries. The numerical scheme successfully reproduces the flow hydrodynamics over rough and highly variable topographies, incorporating an accurate and robust treatment of bore dissipation and the wet and dry process. The method is based on algorithms proposed by Marche et al. (2007), adapted to solve the bed slope source term and to incorporate friction by using the splitting semiimplicit scheme developed by Liang and Marche (2009). An important advantage of this model is the simplicity and low cost of its implementation, yielding accurate results by using coarse computational grids.

Two benchmark test cases are considered to illustrate the capabilities of the new model. Test cases involve the use of dam break floods and boundary fitted grids, with frictional and varying bathymetry. The use of boundary fitted grids is shown for the case of the dam break in a converging–diverging flume (Bellos et al. 1992). Numerical results are in excellent agreement with experimental data obtained by Bellos et al. (1992), showing the ability of the model to address complex geometry and a rapidly varying flow. The process of run-up and run-down, and wetting and drying of the terrain as the wave propagates, are reproduced in the numerical simulations of the benchmark cases analyzed in this investigation. This case also illustrates the stability and the well-balanced property of the current model, because steady state is correctly reached owing to frictional effects.

New experimental data are reported for a dam break wave propagating over the scaled physical model of a river reach with narrow and steep valleys. This experiment is specially designed to test the numerical model and to evaluate its ability to represent extreme and rapid flooding over natural conditions. For this case, the current results have been compared with those from two other NSWE numerical models, showing a better relative performance by the current model in terms of the hydrodynamic variables when similar computational discretizations are employed.

The results reported in this research confirm that the new numerical model is a robust and powerful tool that can be used to simulate high-volume flash floods and significant inundation over dry terrain under realistic conditions, providing accurate results in terms of water depth evolution, discharge, and inundated area. The performance of the model shows that it can become a useful tool for evaluating extreme and rapid flood events over complex bathymetries, and to assess their hazards in terms of inundation extent and depth, depth-averaged velocities, and arrival time of peak discharge. It is expected that the model will be used as an instrument to develop new inundation hazard maps in coastal and riverine areas.

Future research using the model developed in this investigation will focus on the study of complex engineering and geophysical flows. Large-scale coastal flows, such as tsunami propagations (Yamazaki and Cheung 2011), will also be studied by incorporating the Coriolis effect into the model. Also, advanced sediment transport and morphodynamic models (Cao et al. 2004; Vasquez et al. 2008) will be added to the basic equations of the flow to study erosion and sedimentation processes in fluvial and coastal environments. Finally, this model will be employed to investigate density coupled flows, incorporating the transport of active and passive contaminants in rivers and estuaries (Loose et al. 2005).

Appendix. Numerical Simulations of the Dam Break

This section presents additional information about the configuration used for the numerical simulations of the bam break over a physical model using *ANUGA* and *GeoClaw* numerical models. Fig. 11 presents the mesh configuration for each model; Fig. 11(a) presents the triangular mesh of 4,026 required by the *ANUGA* model and Fig. 11(b) presents the initial adaptive mesh used for the simulation with *GeoClaw*. The element size distributions of *ANUGA* and the new model considered approximately 60% of the elements under 100 cm^2 in size, because both distributions are comparable. For the simulation using *GeoClaw*, the time evolution of the distribution of elements is controlled to maintain the number of the finer elements at approximately 4,000, which are 69.4 cm^2 in size. For both models, CFL is equal to 0.95 to achieve numerical stability.

Acknowledgments

This investigation was supported by ECOS-Conicyt project C07U01. Additional support has been provided by Conicyt Fondef project D11i1119 and Conicyt/Fondap program 15110017. The equipment for the laboratory experiments was supplied by the Instituto Nacional de Hidráulica. The authors also thank the technical support provided by Enrique Rosa and the work of Domenico Sciolla and Eduardo González in the development of the experiments.

References

Ahn, T., and Hosoda, T. (2007). "Depth-averaged model of open-channel flows over an arbitrary 3D surface and its applications to analysis of water surface profile." *J. Hydraul. Eng.*, 10.1061/(ASCE)0733-9429(2007)133:4(350), 350–360.

ANUGA [Computer software]. Australian National University and Geoscience Australia, Canberra, Australia.

ASCE. (2006). *Flood resistant design and construction*, Reston, VA.

Audusse, E., Bouchut, F., Bristeau, M., Klein, R., and Benoit, P. (2004). "A fast and stable well-balance scheme with hysdrostatic reconstruction for shallow water flows." *SIAM J. Comput. Sci.*, 25(6), 2050–2065.

Baghlani, A., Talebbeydokhti, N., and Abedini, M. J. (2008). "A shock-capturing model based on flux-vector splitting method in boundary-fitted curvilinear coordinates." *Appl. Math. Model.*, 32(3), 249–266.

Bellos, C., Soulis, J., and Sakkas, J. (1992). "Experimental investigation of two-dimensional dam-break induced flows." *J. Hydraul. Res.*, 30(1), 47–63.

Berger, M., George, D., LeVeque, R., and Mandli, K. (2011). "The Geoclaw software for depth-averaged flows with adaptive refinement." *Adv. Water Resour.*, 34(9), 1195–1206.

Berger, R., and Stockstill, R. (1995). "Finite-element model for high-velocity channels." *J. Hydraul. Eng.*, 10.1061/(ASCE)0733-9429(1995)121:10(710), 710–716.

Berthon, C., and Marche, F. (2008). "A positive preserving high order VFRoe scheme for shallow water equations: A class of relaxation schemes." *SIAM J. Sci. Comput.*, 30(5), 2587–2612.

Bouchut, F. (2004). *Nonlinear stability of finite volume methods for hyperbolic conservation laws*, Basel, Switzerland.

Brufau, P., and García-Navarro, P. (2003). "Unsteady free surface flow simulation over complex topography with multidimensional upwind technique." *J. Comput. Phys.*, 186(2), 503–526.

Brufau, P., Vásquez-Cendón, M., and García-Navarro, P. (2002). "A numerical model for the flooding and drying of irregular domain." *Int. J. Numer. Method. Fluids*, 39(3), 247–275.

Burguete, J., García-Navarro, P., and Murillo, J. (2008). "Friction term discretization and limitation to preserve stability and conservation in the 1D shallow-water model: Application to unsteady irrigation and river flow." *Int. J. Numer. Method. Fluids*, 58(4), 403–425.

Cao, Z., Pender, G., Wallis, S., and Carling, P. (2004). "Computational dam-break hydraulics over erodible sediment bed." *J. Hydraul. Eng.*, 10.1061/(ASCE)0733-9429(2004)130:7(689), 689–703.

Cenderelli, D., and Wohl, E. (2001). "Peak discharge estimates of glacial-lake outburst floods and normal climatic floods in the Mount Everest region, Nepal." *Geomorphology*, 40(1–2), 57–90.

Cienfuegos, R., Barthelemy, E., and Bonneton, P. (2007). "A fourth order compact finite volume scheme for fully nonlinear and weakly dispersive Boussinesq-type equations—Part II: Boundary conditions and validation." *Int. J. Numer. Method. Fluids*, 53(9), 1423–1455.

Clawpack Version 4.6.3 [Computer software]. University of Washington, Clawpack Development Team, Seattle.

Cunge, J., Holly, F., and Verwey, A. (1980). *Practical aspects of computational river hydraulics*, Pitman Publishing, London.

Dussaillant, A., Benito, G., Buytaert, W., Carling, P., Meier, C., and Espinoza, F. (2009). "Repeated glacial-lake outburst floods in Patagonia: An increasing hazard?." *Nat. Hazards*, 54(2), 469–481.

FEMA. (2011). *Coastal construction manual: Principles and practices of planning, siting, designing, constructing, and maintaining residential buildings in coastal areas*, 4th Ed, FEMA, Washington, DC.

Fritz, H., et al. (2011). "Field survey of the 27 February 2010 Chile tsunami." *Pure Appl. Geophys.*, 168(11), 1989–2010.

Gallardo, C., Parés, M., and Castro, M. (2007). "On a well-balanced higher-order finite volume scheme for shallow water equations with topography and dry areas." *J. Comput. Phys*, 227(1), 574–601.

Gallouet, T., Herard, J.-M., and Seguin, N. (2003). "Some approximate Godunov scheme to compute shallow-water equations with topography." *Comput. Fluids*, 32(4), 479–513.

Greenberg, J., and Leroux, A. (1996). "A well-balanced scheme for the numerical processing of source terms in hyperbolic equations." *SIAM J. Numer. Anal.*, 33(1), 1–16.

Hibberd, S., and Peregrine, D. (1979). "Surf and run-up on a beach: A uniform bore." *J. Fluid Mech.*, 95(2), 323–345.

Kawahara, M., and Umetsu, T. (1986). "Finite element method for moving boundary problems in river flow." *Int. J. Numer. Methods Fluids*, 6(6), 365–386.

Lackey, T., and Sotiropoulos, F. (2005). "Role of artificial dissipation scaling and multigrid acceleration in numerical solution of the depth-averaged free-surface flow equations." *J. Hydraul. Eng.*, 10.1061/(ASCE)0733-9429(2005)131:6(476), 476–487.

Lay, L., Ammon, C., Kanamori, H., Koper, K., Sufri, O., and Hutko, A. (2010). "Teleseismic inversion for rupture process of the 27 February 2010 Chile (mw 8.8) earthquake." *Geophys. Res. Lett.*, 37(13), L13301.

LeVeque, R. (1998). "Balancing source terms and flux gradients in high-resolution Godunov methods: The quasi-steady wave-propagation algorithm." *J. Comput. Phys.*, 146(1), 346–365.

LeVeque, R. (2002). *Finite volume methods for hyperbolic problems*, Cambridge University Press, Cambridge, U.K.

Liang, D., Lin, B., and Falconer, R. (2007). "A boundary-fitted numerical model for flood routing with shock-capturing capability." *J. Hydrol.*, 332(3–4), 477–486.

Liang, Q., and Marche, F. (2009). "Numerical resolution of well-balanced shallow water equations with complex source terms." *Adv. Water Resour.*, 32(6), 873–884.

Loose, B., Niño, Y., and Escauriaza, C. (2005). "Finite volume modeling of variable density shallow-water flow equations for a well-mixed estuary: Application to the Rio Maipo estuary in central Chile." *J. Hydraul. Res.*, 43(4), 339–350.

Marche, F., Bonneton, P., Fabrie, P., and Seguin, N. (2007). "Evaluation of well-balance bore-capturing schemes for 2D wetting and drying processes." *Int. J. Numer. Methods Fluids*, 53(5), 867–894.

Masella, J.-M, Faille, I., and Gallouët, T. (1999). "On an approximate godunov scheme." *Int. J. Comput. Fluid Dyn.*, 12(2), 133–149.

Molls, T., and Chaudry, D. (1995). "Depth-averaged open-channel flow model." *J. Hydraul. Eng.*, 10.1061/(ASCE)0733-9429(1995)121:6(453), 453–465.

Molls, T., and Zhao, G. (2000). "Depth-averaged simulation of supercritical flow in channel with wavy sidewall." *J. Hydraul. Eng.*, 10.1061/(ASCE)0733-9429(2000)126:6(437), 437–444.

Mungkasi, S., and Roberts, S. G. (2013). "Validation of ANUGA hydraulic model using exact solutions to shallow water wave problems." *J. Phys.*, 423, 24–25.

Nikolos, I., and Delis, A. (2009). "An unstructured node-centered finite volume scheme for shallow water flows with wet/dry fronts over complex topography." *Comput. Method. Appl. Mech. Eng.*, 198(47–48), 3723–3750.

Saint-Venant, Barré de (1971). "Théorie du mouvement non permanent des eaux, avec application aux crues des rivières et à l'introduction des marées dans leur lit." *C.R. (Comptes Rendus des Séances de l'Académie des Sciences. Paris.)*, 73, 147–154, 237–240.

Sanders, B. (2002). "Non-reflecting boundary flux function for finite volume shallow water models." *Adv. Water Resour.*, 25(2), 195–202.

Stoker, J. (1992). *Water waves, the mathematical theory with applications*, Wiley, New York.

Toro, E. (2001). *Shock-capturing methods for free-surface shallow flows*, Wiley, New York.

Tucciarelli, T., and Termini, D. (2000). "Finite-element modeling of flood-plain flow." *J. Hydraul. Eng.*, 10.1061/(ASCE)0733-9429(2000)126:6(416), 416–424.

Valiani, A., Caleffi, V., and Zanni, A. (2002). "Case study: Malpasset dam-break simulation using a two-dimensional finite volume method." *J. Hydraul. Eng.*, 10.1061/(ASCE)0733-9429(2002)128:5(460), 460–472.

Van Leer, B. (1979). "Toward the ultimate conservative difference scheme V. A second order sequel to Godunov's method." *J. Comput. Phys.*, 32(1), 101–136.

Vasquez, J., Steffler, P., and Millar, R. (2008). "Modeling bed changes in meandering rivers using triangular finite elements." *J. Hydraul. Eng.*, 10.1061/(ASCE)0733-9429(2008)134:9(1348), 1348–1352.

Yamazaki, Y., and Cheung, K. (2011). "Shelf resonance and impact of near field tsunami generated by the 2010 Chile earthquake." *Geophys. Res. Lett.*, 38(12), 12605–12612.

Yeh, H. (1991). "Tsunami bore runup." *Nat. Hazards*, 4(2–3), 209–220.

Yeh, H. (2006). "Maximum fluid forces in the tsunami runup zone." *J. Waterway, Port, Coastal, Ocean Eng.*, 10.1061/(ASCE)0733-950X(2006)132:6(496), 496–500.

Zhou, J., Causon, D., Mingham, C., and Ingram, D. (2004). "Numerical prediction of dam-break flows in general geometries with complex topography." *J. Hydraul. Eng.*, 10.1061/(ASCE)0733-9429(2004)130:4(332), 332–340.